# Femtosecond-Laser-Induced Nanoscale Blisters in Polyimide Thin Films through Nonlinear Absorption

Alan T.K. Godfrey,* Deepak L.N. Kallepalli, Jesse Ratté, Chunmei Zhang,† and P.B. Corkum
*Joint Attosecond Science Laboratory, University of Ottawa and National Research Council of Canada, 25 Templeton Street, Ottawa K1N 6N5, Canada*

(Received 20 April 2020; revised 17 September 2020; accepted 18 September 2020; published 29 October 2020)

Nonlinear absorption of femtosecond laser pulses provides a unique opportunity to confine energy deposition in any medium to a region that is below the focal diameter of a pulse. Illumination of a polymer film through a transparent high-band-gap material such as glass, followed by nonlinear absorption of 800-nm light in polymers, allows us to further restrict absorption to a very thin layer along the propagation direction. We demonstrate this confinement by simulating femtosecond-laser-induced polymer modification by linear, two-photon, and three-photon absorption, and discuss the control over energy absorption in polymers that multiphoton processes offer. Energy deposited in a thin polymer film induces a protruding blister. We present experimental results for blister diameter and height scaling with variation of pulse energy. Using pulse energies of 20–200 nJ and 0.4-NA focusing, we fabricate blisters with diameters of 1–5.5 $\mu$m and heights of 75 nm to 2 $\mu$m. Using 0.95-NA focusing, we obtain laser-induced blisters with diameters as small as 700 nm, suggesting blister-based laser-induced forward transfer is possible on and below the 1-$\mu$m scale. Submicrometer blister formation with use of femtosecond lasers also offers a method of direct, precise laser writing of microstructures on films with single laser pulses. This method is a possible alternative to lithography, laser milling, and laser-based additive machining.

DOI: 10.1103/PhysRevApplied.14.044057

## I. INTRODUCTION

When a femtosecond light pulse irradiates a material, one can easily exceed the ablation threshold of the material, leading to material removal long before heat transport becomes important [1–3]. This enables, for example, deterministic machining, sub-focal-spot machining, and nanoscale fabrication [4–6].

A similar situation can arise for irradiation of a low-band-gap material by light that has passed through a high-band-gap medium. For example, a femtosecond pulse containing approximately $1.3 \times 10^{13}$ W/cm$^2$ can pass through a thick borosilicate glass plate before free-carrier generation in the medium is great enough to significantly attenuate the beam [7]. A few-cycle pulse in fused silica can even reach approximately $10^{14}$ W/cm$^2$ [8]. If high intensities are reached while Kerr-induced self-focusing is avoided (by use of tight focusing [9] or a sufficiently thin medium), a polymer film on glass can experience high-order multiphoton absorption of a well-controlled beam. Furthermore, with a modest increase of intensity above the threshold for free-carrier generation, the primary influence of the glass medium is to cap the intensity but leave the pulse otherwise unchanged in space and time [10].

We study the light-polymer interaction under these conditions. When an intense laser pulse is focused through a substrate onto a coated film, it can create a pocket of superheated material beneath the surface of the film that expands into a protruding blister. Blisters have been used to achieve laser-induced forward transfer, where they impart thrust on an object or material on the surface, thereby desorbing it while avoiding direct laser exposure [11].

Both polymers and metals have been explored as sacrificial laser-absorbing layers for laser-induced-forward-transfer applications, with pulse durations ranging from nanoseconds to femtoseconds [11–16]. Polymer films are ideal for preserving the chemical purity of the transferred material; metals are prone to degradation from thermal and chemical damage, leading to contamination of the transferred material [17]. Arnold and coworkers [11,13,16] demonstrated blister formation by linear absorption of nanosecond lasers in polyimide films. The underlying physics of polymer-blister formation in the nanosecond-pulse regime was addressed for blisters with a width of of 10–100 $\mu$m. However, no thorough studies regarding femtosecond lasers and nonlinear-absorption processes have been performed to our knowledge. Blisters on the few-micrometer and submicrometer scales have also not been explored. Nonlinear absorption of femtosecond pulses

*agodfrey@uottawa.ca
†chunmei.zhang@uottawa.ca

 

leads to confined energy deposition due to thresholdlike absorption behavior and lack of heat dissipation over the timescale of the pulse.

In this paper, we demonstrate the advantages of nonlinear absorption of femtosecond pulses to create polymer blisters. We calculate material breakdown induced by single femtosecond pulses in laboratory conditions to illustrate the confinement of energy deposition. We then show blisters fabricated in polyimide films with use of single femtosecond pulses. We examine the effects of laser pulse energy on the resulting blister size, and show a linear relationship between the energy deposited into the polymer and the resulting blister volume.

This work establishes a method for direct and precise laser writing of microstructures on films using single laser pulses, which is an alternative to lithography, laser milling, and laser-based additive machining. Since the laser energy is deposited beneath the film, morphological changes are achieved while preserving the surface chemistry [18].

## II. EXPERIMENTAL AND CALCULATION DETAILS

### A. Experiment

A schematic of the femtosecond-laser-induced-blister-formation experiment is shown in Fig. 1(a). We use a Coherent RegA 9040 Ti:sapphire laser producing transform-limited pulses with a duration of 45 fs (FWHM, measured via frequency-resolved optical gating [19] by a MesaPhotonics MP002 FROGscan instrument) at a central wavelength of 800 nm. The beam is passed through a spatial filter and the spatial profile is verified to be Gaussian with a beam profiler (DataRay WinCamD UCD12); we measure the beam to have $M^2 = 1.08 \pm 0.02$. We adjust the pulse energy using a rotatable half-wave plate followed by a linear polarizer. The laser beam is focused by a 0.4-NA microscope objective (Edmund Optics DIN

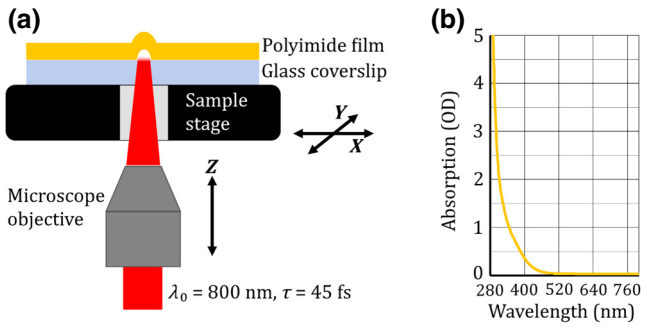


FIG. 1. (a) Experimental configuration. Single femtosecond pulses are focused through a coverslip substrate onto the underside of a polyimide film. (b) Visible linear-absorption spectrum of polyimide film with a thickness of 1.3 $\mu$m. No linear absorption is seen for visible wavelengths longer than 500 nm.

20× 0.4-NA achromatic objective, corrected for 170-$\mu$m coverslips, stock no. 33-438), which is mounted into a vertical motor stage for adjustment of focal-spot placement. The 6-mm aperture of the objective is filled with a 4-mm-diameter beam; therefore, the $1/e^2$ focal-spot diameter is estimated to be $2\omega_0 = (6\,\text{mm}/4\,\text{mm})(1.22\lambda/\eta) \approx 3.7\,\mu$m, where $\eta$ is the NA of the objective [20,21]. We adjust the chirp using a grating compressor to maximize the intensity after the objective, indicated by second-harmonic yield from a $\beta$-barium borate crystal. In one instance, a 0.95-NA objective (Leitz Wetzlar 80× 0.95-NA PL objective, stock no. 48728) with a 10-mm entrance aperture is also used, resulting in an estimated focal-spot diameter of 2.6 $\mu$m. This objective is not coverslip corrected, resulting in spherical aberration that stretches the focus axially and reduces the peak intensity at the focus [22]. Reduced intensity from spherical aberration effects and chirp from additional glass in the 0.95-NA objective is compensated by increasing the pulse energy.

We use polyimide films on no. 1.5 Fisherbrand borosilicate glass coverslips (0.16–0.19 mm in thickness) as substrates, which are prerinsed in acetone, isopropyl alcohol, and deionized water and dried on a hotplate. We calculate the critical power for self-focusing of borosilicate glass at 800 nm to be 2.5 MW [23]; for our 50-fs pulse, this corresponds to a pulse energy of 180 nJ. Focused to a 3-$\mu$m spot size, the light intensity before self-focusing in the substrate occurs can reach $3 \times 10^{13}$ W/cm$^2$ in the absence of nonlinear absorption by the substrate. Films are spin-coated with use of PI-2555 precursor purchased from HD Microsystems at a spin speed of 6000 revolutions/min for 60 s. This yields a film thickness of $1.31 \pm 0.05$ $\mu$m as determined with a Bruker Dektak XT contact profilometer. We measure the linear-absorption spectra of polyimide films from 280 to 800 nm using an Agilent Cary 5000 UV–vis-near-IR spectrophotometer, shown in Fig. 1(b). The films are transparent to wavelengths above 500 nm, indicating that 800-nm light can be absorbed only through two-photon absorption and higher-order processes. The absorption spectra of the polyimide film match the literature and the absorption is ascribed to an $n \rightarrow \pi^*$ transition [24,25].

Above the lens stage, samples are mounted onto a two-axis horizontal stage. Samples are oriented film side up, so that the laser is focused through the coverslip onto the underside of the polyimide film. A dichroic mirror is used before the objective in a coaxial geometry, allowing a small fraction of laser light to be reflected from the sample, recollimated through the objective, and exit to an imaging line for *in situ* laser-spot monitoring. Coupling in white light and changing the position of the objective also allows *in situ* white-light microscopy. We use *in situ* imaging to find the optimal position of the laser focus on the sample. By using pulse energies near the polymer damage threshold at various focal positions, we find that the optimal focal

position corresponds to the blister made with the lowest pulse energy. We rely on optical contrast *in situ*, which is consistent with *ex situ* optical microscope and atomic force microscope (AFM) measurements.

The laser is used in single-shot mode to generate individual blister structures in polyimide films. We characterize the resulting blisters using a JPK Nanowizard II BioAFM instrument in contact mode. From the AFM data, we determine the height, base diameter, and volume of each blister. The blister height is defined as the difference between the local maximum and minimum heights, and the diameter is defined as the effective circular diameter of the base area for each blister. The blister volume is defined as the volume between the elevated surface of a blister and the plane of the flat surroundings at the top surface of the film.

### B. Calculations

To gain a qualitative understanding of the light-polymer interaction, we consider the energy absorption profile when a femtosecond pulse causes laser-induced breakdown through linear, two-photon, and three-photon absorption in a polymer film. Treating each order of absorption separately, we highlight their main features. We assume that the film has the physical characteristics of polyimide ($\rho = 1.42$ g/cm$^3$, $c = 1.09$ J/g K, $T_{\mathrm{decomp}} = 550\,^{\circ}$C) [26,27]. We choose the linear-absorption coefficient to match values used in previous studies on blister formation in polyimide through linear absorption of nanosecond pulses, for comparison with nonlinear absorption [11]. While the heat capacity will not be constant over the temperature range the polymer will experience, we treat it as constant in our qualitative model. Since nonlinear-absorption coefficients of undoped polymers are not reported, we chose two-photon-absorption and three-photon-absorption cross sections to be those of zinc oxide [28]—a material with a similar band gap. We also assume that the laser pulse has a Gaussian temporal profile, with $\tau = 50$ fs being the $1/e$ full width of the intensity in time, and a Gaussian spatial profile with $2\omega_0 = 3$ $\mu$m, where $2\omega_0$ is the $1/e$ full width of the electric field in space. See Supplemental Material [29] for further details of this calculation.

## III. RESULTS AND DISCUSSION

In Fig. 2, we show the calculated temperature profile due to each of the three absorption mechanisms. Pulse energies are chosen such that the peak temperature in the material reaches 10 000 K in all cases. This is the temperature of cold-dense plasmas [30] which is accessible, at least briefly, under normal laboratory conditions. At this temperature we expect molecular dissociation and ionization. Thus, within this assumption, we heat the polymer near the interface (a breakdown depth of approximately 100 nm in the three-photon calculation) until it forms a plasma, transforming its chemical state [18,31–34] in the process.

Figure 2 shows that the heat-deposition region is smaller in all directions for nonlinear absorption. Most notably, the depth of energy deposition is more than 20 times shallower in the case of the three-photon absorption compared with linear absorption, and is approximately two thirds of the diameter. The pulse energy used in this case is also an order of magnitude lower; this is due to the high intensities of tightly focused femtosecond pulses and the cubic intensity dependence of three-photon absorption. Figure 2 also illustrates more general characteristics

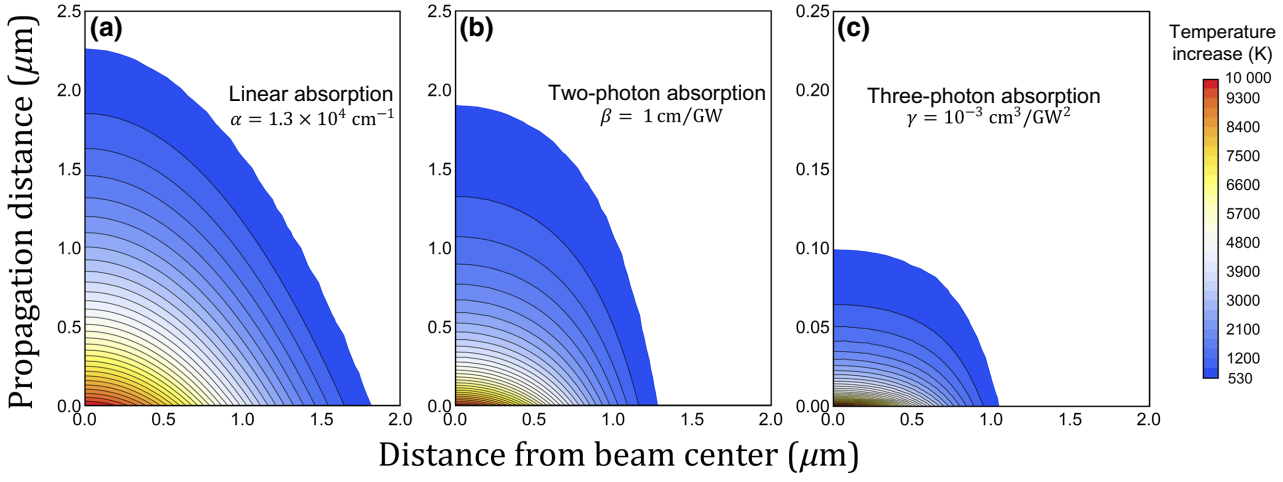


FIG. 2. Calculated temperature distributions induced by a 50-fs laser pulse focused to a 1.5-$\mu$m radius in materials with (a) linear- (polyimide-like) absorption, (b) two-photon- (ZnO-like) absorption, and (c) three-photon- (ZnO-like) absorption mechanisms. Pulse energies of (a) 42 nJ, (b) 31 nJ, and (c) 2.5 nJ are chosen to set the peak temperature to 10 000 K in all cases. The vertical axis for (c) is stretched by a factor of 10.

of energy deposition through high-order nonlinear absorption. After the third-order term dominates (for intensities above $10^{12}$ W/cm$^2$), most of the beam energy is deposited within a very small volume. The penetration depth is very shallow (approximately 100 nm), thereby resulting in precise energy deposition within a thin film. Higher intensity, which leads to higher orders of absorption, will accentuate this trend without changing the overall conclusion. These characteristics should be important for blister-based laser-induced forward transfer of sensitive materials on the nanoscale; energy must be deposited with both lateral and axial confinement to create a nanoscale blister without penetrating and rupturing the film.

Now we move to the experiment. We show that once we exceed an intensity of $3 \times 10^{12}$ W/cm$^2$ (where three-photon absorption dominates in our model), we create blisters with volumes that grow linearly with intensity. For even higher input intensity, this growth slows since intensities above the ionization threshold of the substrate are now attenuated before reaching the polymer [10]. However, we show that by estimating the energy deposited in both the dielectric and the polymer, the linear growth of the blister volume with the energy absorbed by the polymer remains valid.

We first examine the dependence of blister height and diameter on pulse energy. Figure 3 shows AFM scans of blisters created near the blister-formation threshold obtained with a 0.4-NA objective. Along the $X$ direction, four blisters are made at a fixed pulse energy to assess the repeatability of the blister-formation process. Along the $Y$ direction, the pulse energy is varied. We account for losses due to Fresnel reflections from the sample (air-glass and glass-polyimide interfaces) [35]; the net transmission of the sample is 0.954. We observe the blister-formation threshold to be approximately 18 nJ of pulse energy (peak fluence of 0.09 J/cm$^2$, peak intensity of $4 \times 10^{12}$ W/cm$^2$) as measured after losses from the microscope objective. This pulse energy results in a blister of 75-nm height and 1.2-$\mu$m diameter. In our qualitative calculation, a peak temperature of 10 000 K is reached at $3.5 \times 10^{11}$ W/cm$^2$ for three-photon absorption, more than an order of magnitude less intensity than in the two-photon case. The peak intensity at the experimental blister-formation threshold is approximately 20 times that of the three-photon-absorption calculation; at this intensity, three-photon and higher-order processes will dominate over two-photon absorption. Thus, three-photon absorption or higher-order processes are the dominant mechanisms in these experiments.

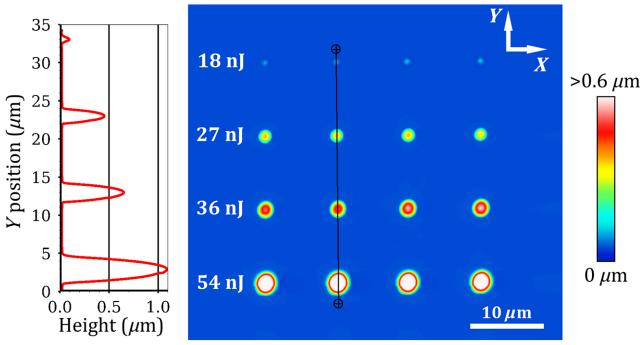


FIG. 3. An AFM image of blisters fabricated in 1.3-$\mu$m polyimide with a 0.4-NA objective with pulse energies near the damage threshold. The AFM line profile displayed (left) corresponds to the cross section denoted by the black line in the two-dimensional image. The blister-formation threshold is seen at a pulse energy of 19 nJ (peak intensity of $4 \times 10^{12}$ W/cm$^2$). Near the threshold, small changes in pulse energy create drastic changes in blister height and diameter.

At low energies, blisters scale strongly in both height and diameter with pulse energy. For example, pulse energies 3 times higher than the threshold result in blisters of 1-$\mu$m height and 3.9-$\mu$m diameter. Figure 4 shows blisters formed in the same conditions but with increased pulse energies. In this regime, blisters have a weaker, linearlike scaling in both height and diameter compared with the strong nonlinear scaling near the threshold. In the rightmost column in Fig. 4, pulse energies of approximately 11 times the threshold energy yield blisters with heights of 2 $\mu$m and base diameters of 5.5 $\mu$m. At such energies, outer parts of the spatial profile of the laser pulses exceed the threshold intensity for blister formation. Some asymmetry in the outer portion of the beam (less than 10% of the peak intensity) is not fully corrected by the spatial filter, resulting in slight but increasing blister asymmetry with increasing pulse energies, as seen in the lower-right portion of blisters in Fig. 4. As the pulse energy is increased above

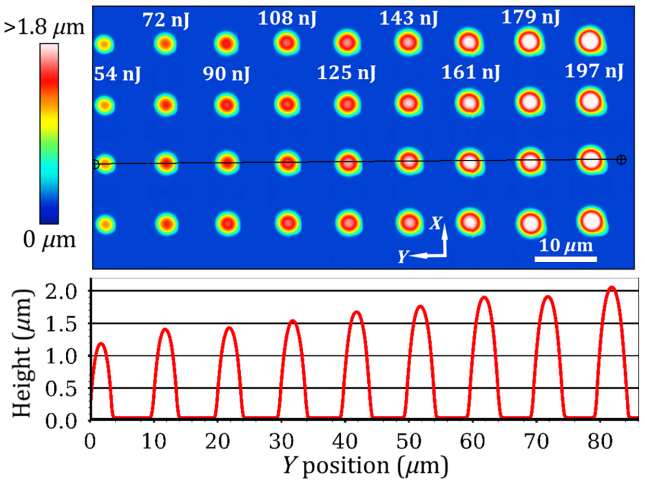


FIG. 4. An AFM image of blisters fabricated in 1.3-$\mu$m polyimide with a 0.4-NA objective with increased pulse energies. The AFM line profile displayed (bottom) corresponds to the cross section denoted by the black line in the two-dimensional image. For intermediate pulse energies, blister heights and diameters scale less steeply with pulse energy.

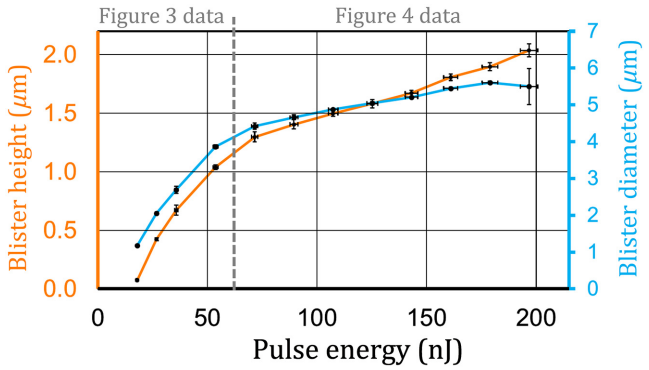


FIG. 5. Dependence of blister height and diameter on pulse energy. As seen in Fig. 3, near-threshold scaling of the height and diameter is nonlinear. At the higher energies shown in Fig. 4, the trend becomes linear until the onset of blister rupture. The horizontal error bars represent pulse-energy variations of the laser.

200 nJ, blisters rupture due to excessive pressure built up beneath the film; they are no longer left intact, showing cracking, diminished height, and removal of material. See Supplemental Material [29] for further details on blister rupture.

Height and diameter scaling for intact blisters in these experiments is summarized in Fig. 5. As also seen directly through AFM images, both scaling curves have two distinct regimes: (i) nonlinear scaling from the threshold pulse energy to 72 nJ and (ii) linearlike scaling onward until the onset of rupture. The monotonic increase of blister height and diameter with pulse energy is consistent with the literature, and is due to increased temperatures and pressures of the material confined beneath the film [16].

Since the laser pulses in these experiments are often intense enough to cause substrate breakdown, we must account for energy lost to the substrate before a pulse reaches the polymer. In these situations, any intensity exceeding the breakdown threshold of the medium is simply removed from the beam to a reasonable approximation [10]. We adopt this model for a Gaussian pulse in both space and time. We estimate the intensity threshold for blister formation as the peak intensity in time at the edge of a blister formed with the threshold pulse energy ($I_{\text{peak}} \approx 3 \times 10^{12}$ W/cm$^2$). We then calculate the energy absorbed in the polymer as a function of the pulse energy used. This decouples the effects of nonlinear optical interactions in glass and polyimide from the expansion process of polyimide blisters.

Figure 6 shows the dependence of blister volume, height, and diameter on energy absorbed in the film, accounting for absorption losses in the substrate. The resulting blister volumes ($V$) shown in Fig. 6(a) are linear with the amount of energy absorbed in the film ($E_{\text{abs}}$). Figure 6(b) shows that the height ($H$) and diameter ($D$) scale approximately with the square root and the fourth root, respectively, of the absorbed pulse energy. Considering that a conical-like volume is proportional to the base area (approximately $\frac{1}{4}\pi D^2$) times the height, the sum of these powers is consistent with the linear trend seen for the blister volume.

We propose a physical reason for the linear trend between blister volume and energy absorbed in the film. Since the laser-induced transition from a solid to a dense plasma is well established at intensities above $3 \times 10^{12}$ W/cm$^2$, from our calculations, we can estimate that most of the pulse energy is used to create the plasma and transport heat. This dense plasma contains many

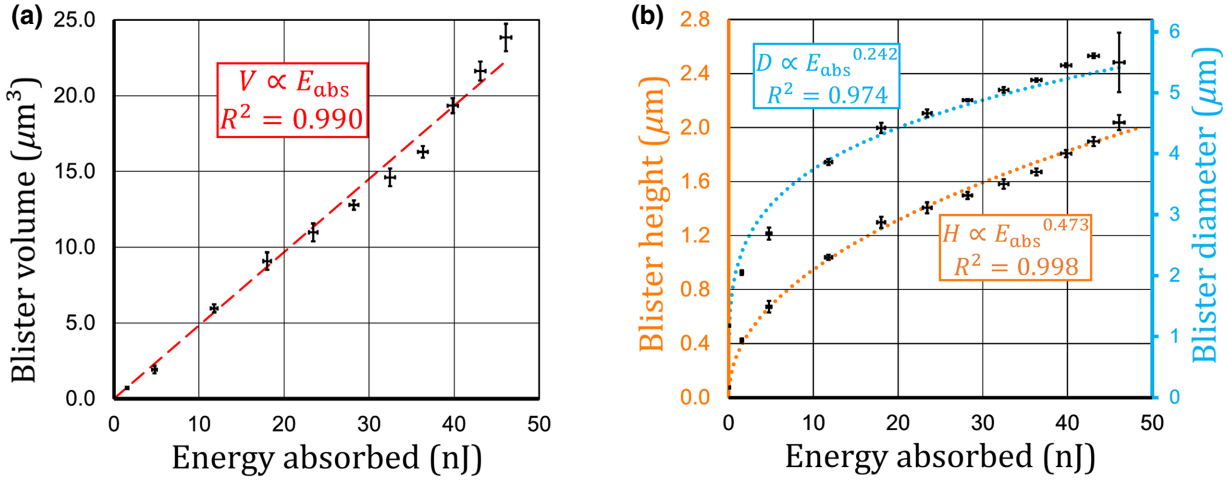


FIG. 6. Dependence of (a) blister volume ($V$) and (b) blister height ($H$) and blister diameter ($D$) on pulse energy absorbed in a 1.3-$\mu$m polyimide film with use of a 0.4-NA objective. The horizontal error bars represent variations in absorbed energy due to pulse-energy variations of the laser. The coefficients of determination ($R^2 \sim 1$) show excellent agreement with the linear fit in (a) and power fits in (b).

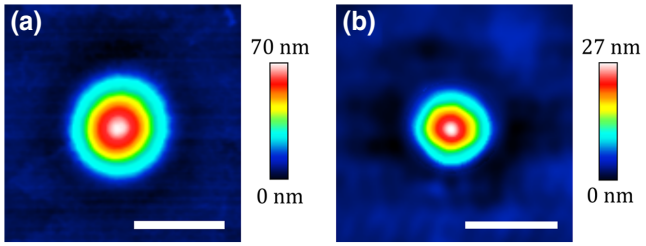


FIG. 7. (a) An AFM image of the smallest observed blister fabricated with a 0.4-NA objective. The $1/e^2$ diameter of the blister is 1.01 $\mu$m, which is 28% of the focal-spot diameter. (b) An AFM image of the smallest observed blister fabricated with a 0.95-NA objective. The $1/e^2$ diameter is 710 nm, which is 28% of the Gaussian focal-spot diameter. The scale bars are 1 $\mu$m wide in both images.

dissociated products, and will also thermally break down the neighboring polymer. Through these processes, many new products are created, some of which are gaseous. As we add more energy, we break proportionally more bonds, which creates proportionally more gas. The gas we create will be at an elevated temperature and pressure but very small in volume. This is followed by rapid isothermal expansion, converting the generated pressure-volume work into a final volume at ambient pressure ($V_F = P_I V_I / P_F$). The linear trend between volume and absorbed energy is consistent with similar experiments involving femtosecond-laser fabrication of voids in fused silica [36]. Since we know the volume of gas created, it should be possible to estimate the time-dependent pressure and therefore the surface motion, which is a measurable quantity.

A powerful consequence of nonlinear absorption is the possibility of energy deposition at scales below the diffraction limit. To understand the resolution advantage of forming blisters through nonlinear absorption, we closely examine AFM images of the smallest blisters formed with 18 nJ of pulse energy and a 0.4-NA objective (as shown in Fig. 3). The smallest of these is shown in Fig. 7(a). The resulting blisters have $1/e^2$ diameters of $1.02 \pm 0.1$ $\mu$m, which is 28% of the focal-spot diameter. The $1/e^2$-diameter definition is used because blister structures have smooth curvature and no distinct cutoff, like the intensity distribution of the Gaussian focal spot used to create them. We also examine the smallest blister made with 160 nJ of pulse energy and a 0.95-NA objective, shown in Fig. 7(b). In this case, a diameter of 710 nm is achieved, which is again 28% of the focal-spot diameter, and is smaller than the laser wavelength.

Looking forward, even smaller structures should be possible. Beyond traditional geometric optics, a key consideration is the thickness of the irradiated film; the resolution limit in subwavelength desorption of thin films decreases significantly with decreasing film thickness [37]. We have calculated, and experimentally shown through helium-ion microscopy and x-ray photoelectron spectroscopy, that the penetration depth into the film becomes very small for high-order nonlinear absorption, which will aid in creating intact blisters in thinner films [18]. Higher orders of nonlinear absorption could also be used to further restrict energy deposition.

## IV. CONCLUSION

Femtosecond laser pulses provide a unique opportunity to deposit energy in a highly controlled manner, through the choice of the absorption mechanism, pulse energy, pulse duration, and substrate mediation via intensity and material choice. Through our calculations, we illustrate the advantage of femtosecond pulses for confining energy deposition in a thin film. We demonstrate this advantage by achieving laser-induced blisters smaller than the laser wavelength. Blister formation at these scales is highly tunable, with resulting blister volumes that scale linearly with the energy deposited in the material.

Further steps could be taken to refine the blister-formation process. For example, a composite film with stacked layers of different materials could be used to control energy deposition and expansion separately, and we could use high-speed surface interferometry to measure the height and velocity of a blister as it expands. In addition, energy deposition will scale linearly with pulse duration for a fixed peak intensity, providing further control over the expansion rate. These techniques would be a convenient way to tailor blister-based laser-induced forward transfer of sensitive materials, where ejection speed is critical.

Precise fabrication of laser-induced blisters could impact several fields. This approach could lead to nanoscale blister-based laser-induced forward transfer of arbitrarily sensitive materials. Blisters on the few-micrometer and submicrometer scales can also be used for direct surface texturing and patterning of materials. Precise microtexturing and perturbation of surfaces can be achieved without lithography, laser milling, or laser-based additive machining. No external processes are used to add or remove materials, and the surface composition remains unchanged since the energy is confined beneath the film [18]. Blister microstructuring of surfaces could find interesting applications in chemically-stable-superhydrophobic-surface patterning and rapid microlens-array fabrication. Blisters may also be used to create metamaterials by directly writing subwavelength surface structures.

## ACKNOWLEDGMENTS

We acknowledge Dr. Maohui Chen for training in atomic force microscopy and Tony Olivieri for training related to polyimide-film fabrication. We are also pleased

to acknowledge the support of laboratory engineers Yu-Hsuan Wang and Tyler Clancy from the University of Ottawa throughout this work. We acknowledge funding from Natural Sciences and Engineering Research Council of Canada (NSERC) Engage (Grant No. EGP 523138-18) and Discovery (Grant No. RGPIN-2019-04603) grants, the Ontario Centres of Excellence Voucher for Innovation and Productivity I Program (Grant No. 29119), Fluidigm Canada, and the Canada Foundation for Innovation. A.T.K.G. acknowledges financial support from the NSERC's Postgraduate Scholarship – Doctoral and the University of Ottawa's Excellence Scholarship.

[1] B. N. Chichkov, C. Momma, S. Nolte, F. von Alvensleben, and A. Tünnermann, Femtosecond, picosecond and nanosecond laser ablation of solids, Appl. Phys. A **63**, 109 (1996).
[2] K. Sugioka and Y. Cheng, Ultrafast lasers-reliable tools for advanced materials processing, Light: Sci. Appl. **3**, e149 (2014).
[3] M. Malinauskas, A. Žukauskas, S. Hasegawa, Y. Hayasaki, V. Mizeikis, R. Buividas, and S. Juodkazis, Ultrafast laser processing of materials: From science to industry, Light: Sci. Appl. **5**, e16133 (2016).
[4] A. Joglekar, H. Liu, G. Spooner, E. Meyhfer, G. Mourou, and A. Hunt, A study of the deterministic character of optical damage by femtosecond laser pulses and applications to nanomachining, Appl. Phys. B **77**, 25 (2003).
[5] P. P. Pronko, S. K. Dutta, J. Squier, J. V. Rudd, D. Du, and G. Mourou, Machining of sub-micron holes using a femtosecond laser at 800 nm, Opt. Commun. **114**, 106 (1995).
[6] K. Sugioka and Y. Cheng, Femtosecond laser three-dimensional micro- and nanofabrication, Appl. Phys. Rev. **1**, 041303 (2014).
[7] A. Ben-Yakar and R. L. Byer, Femtosecond laser ablation properties of borosilicate glass, J. Appl. Phys. **96**, 5316 (2004).
[8] M. Lenzner, J. Krüger, S. Sartania, Z. Cheng, C. Spielmann, G. Mourou, W. Kautek, and F. Krausz, Femtosecond Optical Breakdown in Dielectrics, Phys. Rev. Lett. **80**, 4076 (1998).
[9] N. T. Nguyen, A. Saliminia, W. Liu, S. L. Chin, and R. Valle, Optical breakdown versus filamentation in fused silica by use of femtosecond infrared laser pulses, Opt. Lett. **28**, 1591 (2003).
[10] D. M. Rayner, A. Naumov, and P. B. Corkum, Ultrashort pulse non-linear optical absorption in transparent media, Opt. Express **13**, 3208 (2005).
[11] N. T. Kattamis, P. E. Purnick, R. Weiss, and C. B. Arnold, Thick film laser induced forward transfer for deposition of thermally and mechanically sensitive materials, Appl. Phys. Lett. **91**, 171120 (2007).
[12] P. Delaporte and A.-P. Alloncle, Laser-induced forward transfer: A high resolution additive manufacturing technology, Opt. Laser Technol. **78**, 33 (2016).
[13] M. S. Brown, C. F. Brasz, Y. Ventikos, and C. B. Arnold, Impulsively actuated jets from thin liquid films for high-resolution printing applications, J. Fluid Mech. **709**, 341 (2012).
[14] N. T. Goodfriend, S. Y. Heng, O. A. Nerushev, A. V. Gromov, A. V. Bulgakov, M. Okada, W. Xu, R. Kitaura, J. Warner, H. Shinohara, and E. E. B. Campbell, Blister-based-laser-induced-forward-transfer: A non-contact, dry laser-based transfer method for nanomaterials, Nanotechnology **29**, 385301 (2018).
[15] A. Piqué, H. Kim, and C. B. Arnold, in *Laser Ablation and its Applications*, Springer Series in Optical Sciences, edited by C. Phipps (Springer, US, Boston, MA, 2007), p. 339.
[16] M. S. Brown, N. T. Kattamis, and C. B. Arnold, Time-resolved study of polyimide absorption layers for blister-actuated laser-induced forward transfer, J. Appl. Phys. **107**, 083103 (2010).
[17] N. T. Kattamis, N. D. McDaniel, S. Bernhard, and C. B. Arnold, Laser direct write printing of sensitive and robust light emitting organic molecules, Appl. Phys. Lett. **94**, 103306 (2009).
[18] D. L. N. Kallepalli, A. T. K. Godfrey, J. Walia, F. Variola, A. Staudte, C. Zhang, Z. J. Jakubek, and P. B. Corkum, Multiphoton laser-induced confined chemical changes in polymer films, Opt. Express **28**, 11267 (2020).
[19] R. Trebino, K. W. DeLong, D. N. Fittinghoff, J. N. Sweetser, M. A. Krumbgel, B. A. Richman, and D. J. Kane, Measuring ultrashort laser pulses in the time-frequency domain using frequency-resolved optical gating, Rev. Sci. Instrum. **68**, 3277 (1997).
[20] O. H. Y. Zalloum, M. Parrish, A. Terekhov, and W. Hofmeister, On femtosecond micromachining of HPHT single-crystal diamond with direct laser writing using tight focusing, Opt. Express **18**, 13122 (2010).
[21] K. Sugioka, Progress in ultrafast laser processing and future prospects, Nanophotonics **6**, 393 (2016).
[22] L. Capuano, R. Pohl, R. M. Tiggelaar, J. W. Berenschot, J. G. E. Gardeniers, and G. R. B. E. Römer, Morphology of single picosecond pulse subsurface laser-induced modifications of sapphire and subsequent selective etching, Opt. Express **26**, 29283 (2018).
[23] C. B. Schaffer, A. Brodeur, and E. Mazur, Laser-induced breakdown and damage in bulk transparent materials induced by tightly focused femtosecond laser pulses, Meas. Sci. Technol. **12**, 1784 (2001).
[24] M. Nishikawa, B. Taheri, and J. L. West, Mechanism of unidirectional liquid-crystal alignment on polyimides with linearly polarized ultraviolet light exposure, Appl. Phys. Lett. **72**, 2403 (1998).
[25] B. Li, T. He, and M. Ding, Tuning the aggregation of polyimide thin films by modification of their molecular interactions, Polym. Int. **49**, 395 (2000).
[26] DuPont Kapton – Summary of Properties.
[27] PRODUCT BULLETIN – PI 2525, PI 2555 & PI 2574 (2012).
[28] M. G. Vivas, T. Shih, T. Voss, E. Mazur, and C. R. Mendonca, Nonlinear spectra of ZnO: Reverse saturable, two- and three-photon absorption, Opt. Express **18**, 9628 (2010).
[29] See Supplemental Material at http://link.aps.org/supplemental/10.1103/PhysRevApplied.14.044057 for further

details on blister-rupture and temperature-distribution calculations.

[30] S. H. Glenzer, O. L. Landen, P. Neumayer, R. W. Lee, K. Widmann, S. W. Pollaine, R. J. Wallace, G. Gregori, A. Höll, T. Bornath, R. Thiele, V. Schwarz, W.-D. Kraeft, and R. Redmer, Observations of Plasmons in Warm Dense Matter, Phys. Rev. Lett. **98**, 065002 (2007).

[31] D. L. N. Kallepalli, A. M. Alshehri, D. T. Marquez, L. Andrzejewski, J. C. Scaiano, and R. Bhardwaj, Ultra-high density optical data storage in common transparent plastics, Sci. Rep. **6**, 26163 (2016).

[32] K. L. N. Deepak, R. Kuladeep, S. Venugopal Rao, and D. Narayana Rao, Luminescent microstructures in bulk and thin films of PMMA, PDMS, PVA, and PS fabricated using femtosecond direct writing technique, Chem. Phys. Lett. **503**, 57 (2011).

[33] Z. Nie, H. Lee, H. Yoo, Y. Lee, Y. Kim, K.-S. Lim, and M. Lee, Multilayered optical bit memory with a high signal-to-noise ratio in fluorescent polymethylmethacrylate, Appl. Phys. Lett. **94**, 111912 (2009).

[34] A. M. Alshehri, K. L. N. Deepak, D. T. Marquez, S. Desgreniers, and V. R. Bhardwaj, Localized nanoclusters formation in PDMS upon irradiation with femtosecond laser, Opt. Mater. Express **5**, 858 (2015).

[35] T. J.-Y. Derrien, R. Koter, J. Krüger, S. Höhm, A. Rosenfeld, and J. Bonse, Plasmonic formation mechanism of periodic 100-nm-structures upon femtosecond laser irradiation of silicon in water, J. Appl. Phys. **116**, 074902 (2014).

[36] E. G. Gamaly, L. Rapp, V. Roppo, S. Juodkazis, and A. V. Rode, Generation of high energy density by fs-laser-induced confined microexplosion, New J. Phys. **15**, 025018 (2013).

[37] V. Sametoglu, V. T. K. Sauer, and Y. Y. Tsui, Production of 70-nm Cr dots by laser-induced forward transfer, Opt. Express **21**, 18525 (2013).